HEAT AND MASS TRANSFER EFFECTS ON THE PERISTALTIC FLOW OF SISKO FLUID IN A CURVED CHANNEL

by

Raheel AHMED**, Nasir ALI, and Khurram JAVID
Department of Mathematics and Statistics, IIU, Islamabad, Pakistan

Original scientific paper
https://doi.org/10.2298/TSCI161018115A

In the present study heat and mass transfer phenomena in flow of non-Newtonian Sisko fluid induced by peristaltic activity through a curved channel have been investigated numerically using an implicit finite difference scheme. The governing equations are formulated in terms of curvilinear co-ordinates with appropriate boundary conditions. Numerically solution is carried out under long wavelength and low Reynolds number assumptions. The velocity field, pressure rise per wavelength, stream function, temperature, and concentration fields have been analyzed for the effects of curvature parameter, viscosity parameter, and power law index. Additionally, the computation for heat transfer coefficient and Sherwood number carried out for selected thermophysical parameters. The main results that are extracted out this study is that for strong shear-thinning biofluids (power-law rheological index, $n < 1$) the flow exhibits the boundary-layer character near the boundary walls. Both temperature and mass concentration are found to increase with increasing the generalized ratio of infinite shear rate viscosity to the consistency index. The amplitude of heat transfer coefficient and Sherwood number is also an increasing function of generalized ratio of infinite shear rate viscosity to the consistency index.

Key words: *peristalsis, heat coefficient, Sherwood number, curved channel*

Introduction

Peristaltic pumping is a phenomena of fluid transport which is achieved through a progressive dynamic waves of contraction or expansion propagating along the walls of a distensible tube containing fluids. It is an inherent phenomena of numerous biological/physiological mechanism such as the male reproductive tract, the movement of chyme in the gastrointestinal tract and fluids from the mouth through the esophagus. Other industrial and physiological applications include roller and finger pumps, dialysis machines, *etc.* Recently, electro osmosis-modulated peristaltic transport in micro-fluids channel is proposed as a model for the design of lab-on-a-chip device [1, 2]. Due to wide range applications, mathematical modelling of peristaltic movement has received increasing interest among researchers. The fundamental work carried out by Latham [3] and Shapiro *et al.* [4] for tube and channel geometry theoretically evaluate the reflux and trapping phenomena associated with peristaltic mechanism under long wavelength and low Reynolds number assumptions. The flow was investigated in the wave frame. Fung and Yih [5] adopted an alternative approach based on perturbation technique to analyze the peristaltic flow in the fixed frame (without employing long wavelength and low Reynolds

* Corresponding author, e-mail: raheel_rwp@yahoo.com

number approximations). The reflux phenomenon was discussed for several values of Reynolds number. Peristaltic flow in a circular tube under long wavelength approximation was proposed as a model of intestinal flow by Barton and Raynor [6]. Later developments in the realm of peristaltic flow was made by several researchers.

Inertial and streamline curvature effects were integrated in the study of peristaltic transport by Jaffrin [7]. A comprehensive review of initial theoretical and experimental work on peristaltic transport was reviewed by Jaffrin and Shapiro [8]. Poiseuille flow with superimposed peristaltic flow was investigated by Mittra and Parsad [9] and Srivastava and Srivastava [10]. Numerical study of 2-D peristaltic flows was carried out by Brown and Hung [11], Takabatake and Ayukawa [12], and Takabatake *et al.* [13]. Non-Newtonian effect on peristaltic mechanism were described by Raju and Devanathan [14] using power law model. Later viscoelastic effects in peristaltic transport using a simple fluid with fading memory were introduced by Raju and Devanathan [15]. Peristaltic pumping of second order fluid in planar channel and tube was discussed by Siddiqui *et al.* [16] and Siddiqui and Schwarz [17]. Hayat *et al.* [18] extended the analysis of peristaltic flow for a third order fluid. Peristaltic flows of Johnson-Segalman and Oldroyd-B model were also investigated by Hayat *et al.* [19, 20]. Srinivasacharya *et al.* [21] investigated the peristaltic transport of micropolar fluid. Mekheimer [22], Haroun [23], Vajravelu *et al.* [24], Tripathi *et al.* [25], Tripathi and Beg [26, 27], Nabil *et al.* [28], Tanveer *et al.* [29], also contributed to the literature on peristaltic transport in various scenarios. A variational method for optimizing peristaltic transport in a channel was presented by Walker and Shelley [30]. Ceniceros and Fisher [31] employed immersed boundary method to study peristaltic flow in a pump for all possible occlusion ratios and Weissenberg number in excess of 100. Boehme and Mueller [32] performed an asymptotic analysis of axisymmetric 2-D peristaltic flow to investigate the influence of the aspect ratio, the Weissenberg number, the Deborah number and the wave shape on the pumping characteristics. Shit and Ray [33] studied effects of applied electric field on hydro-magnetic peristaltic flow through a micro-channel. Abbas *et al.* [34] analyzed peristaltic flow of a hyperbolic tangent fluid in a non-uniform channel in the absence of inertial effects. The investigation of MHD peristaltic blood flow of nanofluid in non-uniform channel is also carried out by Abbas *et al.* [35]. More recently, Abbas *et al.* [36] studied entropy generation in peristaltic flow of nanofluids in a non-uniform 2-D channel with compliant walls.

The analysis carried out in previously mentioned studies do not take into account the curvature effect induced by the geometry of the channel/tube. The first comprehensive attempt which includes curvature effects on peristaltic flow was made by Sato *et al.* [37]. The analysis of Sato *et al.* [37] was extended for a non-Newtonian third grade fluid by Ali *et al.* [38]. Later studies in this area were carried out by Hayat *et al.* [39], Ramanamurthy *et al.* [40], and Kalantari *et al.* [41].

When heat and mass transfer occur simultaneously in a moving fluid, then it affect many transport processes present in nature and also the applications relating to science and engineering. Mass transfer phenomenon is vital in the diffusion process such as the nutrients diffuse out from the blood to the contiguous tissues. Research on bioheat transfer discusses the heat and mass transfer in organisms. Studies pertaining to heat/mass transfer in peristaltic flows have also been carried out by various researchers. This is because of numerous applications of heat/mass transfer in industrial and physiological process like condensation, crystallization, evaporation, *etc.* The literature on peristaltic flows with heat/mass transfer straighter geometries is extensive but very little is said about peristalsis in heated curved channel. Ali *et al.* [42] investigated peristaltic flow in a channel with heated wall for the first time. Later attempts in this direction were made by Hayat *et al.* [43], and Hina *et al.* [44]. However, thus far no attempt is available dealing with peristaltic flow with heat and mass transfer of Sisko fluid in a curved channel. Sisko fluid falls in the category of generalized Newtonian fluids capable of predicting shear-thinning, Newtonian and shear-thickening behaviors. The model is already used by several other researchers in peristaltic and boundary-layer flows in straighter geometries [45].

Mathematical formulation and rheological constitutive equations

Let the channel of width $2a$ is coiled in a circle of radius, R, with center O. An incompressible Sisko fluid is assumed inside the channel. Let the walls of the channel are performing peristaltic motion due to propagation of sinusoidal waves of speed, c, and amplitude, b. It is further assumed that both the walls of channel are maintained at constant temperature. The mass concentration at the both walls is also assumed constant. The flow geometry is explained in fig. 1. A curvilinear co-ordinates (R, X), (in which R is oriented along radial direction and X is along the flow direction,) is employed at the center O for development of flow analysis. The wall surfaces is described by the expressions:

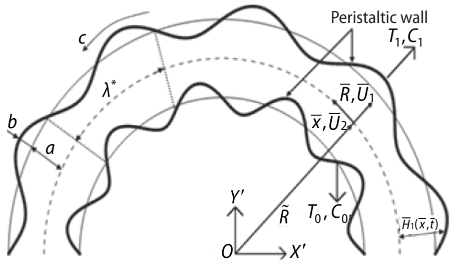

Figure 1. Physical problem of peristaltic flow regime

$$H_1(X,t) = a + b\sin\left[\left(\frac{2\pi}{\lambda^*}\right)(X-ct)\right], \qquad \text{upper wall} \tag{1}$$

$$H_2(X,t) = -a - b\sin\left[\left(\frac{2\pi}{\lambda^*}\right)(X-ct)\right], \qquad \text{lower wall} \tag{2}$$

where λ^* is the wavelength, b – the amplitude, and t – the time.

The fundamental equations which govern the flow are [28, 29]:

– continuity equation

$$\nabla \mathbf{U} = 0 \tag{3}$$

– momentum equation

$$\rho \frac{\mathrm{d}\mathbf{U}}{\mathrm{d}t} = \nabla \boldsymbol{\tau} \tag{4}$$

– energy equation

$$\rho c_p \frac{\mathrm{d}T}{\mathrm{d}t} = k^* \nabla^2 T + \mu \Phi \tag{5}$$

– mass concentration equation

$$\frac{\mathrm{d}C}{\mathrm{d}t} = D\nabla^2 C + \frac{DK_T}{T_m}\nabla^2 T \tag{6}$$

where $\boldsymbol{\tau}$, T, C, c_p, k^*, D, K_T, T_m, Φ, and ρ are the Cauchy stress tensor, temperature, mass concentration, specific heat at constant pressure, thermal conductivity (assumed constant), coefficient of mass diffusivity, thermal diffusivity, mean temperature, dissipation function, and the fluid density, respectively.

The Cauchy stress tensor $\boldsymbol{\tau}$ is given:

$$\boldsymbol{\tau} = -P\mathbf{I} + \mathbf{S} \tag{7}$$

where P is the pressure, $\mathbf{I}$ – the identity tensor, and $\mathbf{S}$ – the extra stress tensor which for *Sisko fluid model* [45, 46] satisfies:

$$\mathbf{S} = \left[a_1 + b_1 (\Pi)^{n-1}\right]\mathbf{A}_1 \tag{8}$$

where a_1 is the infinite shear-rate viscosity, b_1 is the consistency, n is the power-law index, and Π is defined:

$$\Pi = \sqrt{\frac{1}{2}\text{trac}\left(\dot{\gamma}\dot{\gamma}^t\right)} \tag{9}$$

where $\dot{\gamma} = \nabla U + (\nabla U)^t$.

In view of eq. (7), we can write eq. (4):

$$\rho\frac{\mathrm{d}\mathbf{U}}{\mathrm{d}t} = -\nabla P + \nabla\mathbf{S} \tag{10}$$

Assuming $\mathbf{V} = [U_1(X,R,t), U_2(X,R,t), 0]$, $T = T(X,R,t)$, $C = C(X,R,t)$, eqs. (3)-(6) yield:

$$\frac{\partial}{\partial R}\left[\left(R+\tilde{R}\right)U_1\right] + \tilde{R}\frac{\partial U_2}{\partial X} = 0 \tag{11}$$

$$\rho\left(\frac{\partial U_1}{\partial t} + V_1\frac{\partial U_1}{\partial R} + \frac{RU_2}{R+\tilde{R}}\frac{\partial U_1}{\partial X} - \frac{{U_2}^2}{R+\tilde{R}}\right) = -\frac{\partial P}{\partial R} + \frac{1}{R+\tilde{R}}\frac{\partial}{\partial R}\left[\left(R+\tilde{R}\right)S_{RR}\right] + $$
$$+\frac{\tilde{R}}{R+\tilde{R}}\frac{\partial}{\partial X}S_{RX} - \frac{S_{XX}}{R+\tilde{R}} \tag{12}$$

$$\rho\left(\frac{\partial U_2}{\partial t} + V_1\frac{\partial U_2}{\partial R} + \frac{\tilde{R}U_2}{R+\tilde{R}}\frac{\partial U_2}{\partial X} - \frac{U_2U_1}{R+\tilde{R}}\right) = -\left(\frac{\tilde{R}}{R+\tilde{R}}\right)\frac{\partial P}{\partial X} +$$
$$+\frac{1}{\left(R+\tilde{R}\right)^2}\frac{\partial}{\partial R}\left[\left(R+\tilde{R}\right)^2 S_{RX}\right] + \frac{\tilde{R}}{R+\tilde{R}}\frac{\partial}{\partial X}S_{XX} \tag{13}$$

$$\rho c_p\left(\frac{\partial T}{\partial t} + U_1\frac{\partial T}{\partial R} + \frac{\tilde{R}U_2}{R+\tilde{R}}\frac{\partial T}{\partial X}\right) = k^*\left\{\frac{1}{\left(R+\tilde{R}\right)}\frac{\partial}{\partial R}\left[\left(R+\tilde{R}\right)\frac{\partial T}{\partial R}\right] + \left(\frac{\tilde{R}}{R+\tilde{R}}\right)^2\frac{\partial^2 T}{\partial X^2}\right\} +$$
$$+S_{RR}\frac{\partial U_1}{\partial R} + S_{RX}\left(\frac{\partial U_2}{\partial R} + \frac{\tilde{R}}{R+\tilde{R}}\frac{\partial U_1}{\partial X} + \frac{\tilde{R}}{R+\tilde{R}}\frac{\partial U_2}{\partial X} - \frac{U_2}{R+\tilde{R}}\right) +$$
$$+S_{XX}\left(\frac{U_1}{R+\tilde{R}} + \frac{\tilde{R}}{R+\tilde{R}}\frac{\partial U_2}{\partial X}\right) \tag{14}$$

$$\left(\frac{\partial}{\partial t}+U_1\frac{\partial}{\partial R}+\frac{RU_2}{R+\tilde{R}}\frac{\partial}{\partial X}\right)C=D\left[\frac{\partial^2}{\partial R^2}+\frac{\tilde{R}}{R+\tilde{R}}\frac{\partial}{\partial R}+\left(\frac{\tilde{R}}{R+\tilde{R}}\right)^2\frac{\partial^2}{\partial X^2}\right]C+$$

$$+\frac{DK_T}{T_m}\left[\frac{\partial^2 T}{\partial R^2}+\frac{\tilde{R}}{R+\tilde{R}}\frac{\partial T}{\partial R}+\left(\frac{\tilde{R}}{R+\tilde{R}}\right)^2\frac{\partial^2 T}{\partial X^2}\right] \tag{15}$$

where S_{RR}, S_{RX}, and S_{XX} are the components of extra stress. The boundary conditions associated with eqs. (11)-(15) are:

$$U_2=0,\quad U_1=\frac{\partial H_1}{\partial t},\quad T=T_0,\quad C=C_0\quad \text{at}\quad \eta=h_1=1+\lambda\sin x \tag{16}$$

$$U_2=0,\quad U_1=\frac{\partial H_2}{\partial t},\quad T=T_1,\quad C=C_1\quad \text{at}\quad \eta=h_2=-1-\lambda\sin x \tag{17}$$

Transform our flow model from the fixed frame (R, X) to wave frame (r, x) by using transformation:

$$x=X-ct,\quad r=R,\quad p=P,\quad u_1=U_1,\quad u_2=U_2-c,\quad T=T \tag{18}$$

After above transformations, the governing equations in the wave frame become:

$$\frac{\partial}{\partial r}\left[\left(r+\tilde{R}\right)u_1\right]+\tilde{R}\frac{\partial u_2}{\partial x}=0 \tag{19}$$

$$\rho\left[-c\frac{\partial u_1}{\partial x}+u_1\frac{\partial u_1}{\partial r}+\frac{\tilde{R}(u_2+c)}{r+\tilde{R}}\frac{\partial u_1}{\partial x}-\frac{(u_2+c)^2}{r+\tilde{R}}\right]=-\frac{\partial p}{\partial r}+\frac{1}{r+\tilde{R}}\frac{\partial}{\partial r}\left[\left(r+\tilde{R}\right)S_{rr}\right]+$$

$$+\frac{\tilde{R}}{r+\tilde{R}}\frac{\partial}{\partial x}S_{rx}-\frac{S_{xx}}{r+\tilde{R}} \tag{20}$$

$$\rho\left[-c\frac{\partial u_2}{\partial x}+u_1\frac{\partial u_2}{\partial r}+\frac{\tilde{R}(u_2+c)}{r+\tilde{R}}\frac{\partial u_2}{\partial x}-\frac{(u_2+c)u_1}{r+\tilde{R}}\right]=-\left(\frac{\tilde{R}}{r+\tilde{R}}\right)\frac{\partial p}{\partial x}+$$

$$+\frac{1}{\left(r+\tilde{R}\right)^2}\frac{\partial}{\partial r}\left[\left(r+\tilde{R}\right)^2S_{rx}\right]+\frac{\tilde{R}}{r+\tilde{R}}\frac{\partial}{\partial x}S_{xx} \tag{21}$$

$$\rho c_p\left[-c\frac{\partial T}{\partial x}+u_1\frac{\partial T}{\partial r}+\frac{\tilde{R}(u_2+c)}{r+\tilde{R}}\frac{\partial T}{\partial x}\right]=k^*\left\{\frac{1}{\left(r+\tilde{R}\right)}\frac{\partial}{\partial r}\left[\left(r+\tilde{R}\right)\frac{\partial T}{\partial r}\right]+\left(\frac{\tilde{R}}{r+\tilde{R}}\right)^2\frac{\partial^2 T}{\partial x^2}\right\}+$$

$$+S_{rr}\frac{\partial u_1}{\partial r}+S_{rx}\left[\frac{\partial u_2}{\partial r}+\frac{\tilde{R}}{r+\tilde{R}}\frac{\partial u_1}{\partial x}+\frac{\tilde{R}}{r+\tilde{R}}\frac{\partial u_2}{\partial x}-\frac{(u_2+c)}{r+\tilde{R}}\right]+S_{xx}\left(\frac{u_1}{r+\tilde{R}}+\frac{\tilde{R}}{r+\tilde{R}}\frac{\partial u_2}{\partial x}\right) \tag{22}$$

$$\left[-c\frac{\partial}{\partial x}+u_1\frac{\partial}{\partial r}+\frac{\tilde{R}(u_2+c)}{r+\tilde{R}}\frac{\partial}{\partial x}\right]C=D\left[\frac{\partial^2}{\partial r^2}+\frac{1}{r+\tilde{R}}\frac{\partial}{\partial r}+\left(\frac{\tilde{R}}{r+\tilde{R}}\right)^2\frac{\partial^2}{\partial x^2}\right]C+$$

$$+\frac{DK_T}{T_m}\left[\frac{\partial^2 T}{\partial r^2}+\frac{1}{r+\tilde{R}}\frac{\partial T}{\partial r}+\left(\frac{\tilde{R}}{r+\tilde{R}}\right)^2\frac{\partial^2 T}{\partial x^2}\right] \tag{23}$$

The following dimensionless variables are defined to render the previous equations in normalized form:

$$\left.\begin{array}{l}\bar{x}=\dfrac{2\pi}{\lambda^*}x,\ \eta=\dfrac{r}{a_1},\ \bar{u}_1=\dfrac{u_1}{c},\ \bar{u}_2=\dfrac{u_2}{c},\ \mathrm{Re}=\dfrac{\rho c a_1}{\mu},\ \bar{p}=\dfrac{2\pi a_1{}^2}{\lambda^*\mu c}p,\ \delta=\dfrac{2\pi a_1}{\lambda^*},\ \bar{\mathbf{S}}=\dfrac{a_1}{\mu c}\mathbf{S}\\ k=\dfrac{\tilde{R}}{a_1},\ \theta=\dfrac{T-T_1}{T_0-T_1},\ \mathrm{Br}=\dfrac{\mu c^2}{k^*\left(T_0-T_1\right)},\ \phi=\dfrac{C-C_1}{C_0-C_1},\ a^*=\dfrac{a_1}{\mu},\ \mu=\dfrac{b_1}{\left(\dfrac{a_1}{c}\right)^{n-1}}\end{array}\right\} \tag{24}$$

After using these dimensionless variables apply the long wavelength and low Reynolds approximations then eqs. (24) in terms of stream function define:

$$u_1=\delta\frac{k}{\eta+k}\frac{\partial\psi}{\partial x},\ u_2=-\frac{\partial\psi}{\partial\eta}$$

will contract to:

$$\frac{\partial p}{\partial\eta}=0 \tag{25}$$

$$-\frac{\partial p}{\partial x}+\frac{1}{k(k+\eta)}\frac{\partial}{\partial\eta}\left[(k+\eta)^2 S_{x\eta}\right]=0 \tag{26}$$

$$\frac{1}{(k+\eta)}\frac{\partial}{\partial\eta}\left[(k+\eta)\frac{\partial\theta}{\partial\eta}\right]+\mathrm{Br}\,S_{x\eta}\left[-\frac{1}{k+\eta}\left(1-\frac{\partial\psi}{\partial\eta}\right)-\frac{\partial^2\psi}{\partial\eta^2}\right]=0 \tag{27}$$

$$\left[\frac{\partial^2\phi}{\partial\eta^2}+\frac{1}{(k+\eta)}\frac{\partial\phi}{\partial\eta}\right]=-\mathrm{Sr}\,\mathrm{Sc}\left[\frac{\partial^2\theta}{\partial\eta^2}+\frac{1}{(k+\eta)}\frac{\partial\theta}{\partial\eta}\right] \tag{28}$$

$$S_{xx}=0 \tag{29}$$

$$S_{x\eta}=\left[a^*+(\Pi)^{n-1}\right]\left[-\frac{\partial^2\psi}{\partial\eta^2}-\frac{1}{\eta+k}\left(1-\frac{\partial\psi}{\partial\eta}\right)\right] \tag{30}$$

$$S_{\eta\eta}=0 \tag{31}$$

$$\Pi=-\frac{\partial^2\psi}{\partial\eta^2}-\frac{1}{\eta+k}\left(1-\frac{\partial\psi}{\partial\eta}\right) \tag{32}$$

Inserting eq. (30) into eqs. (26) and (27), we get:

$$-\frac{\partial p}{\partial x}+\frac{1}{k(k+\eta)}\frac{\partial}{\partial\eta}\left\{(k+\eta)^2\left[a^*+(\Pi)^{n-1}\right]\left[-\frac{\partial^2\psi}{\partial\eta^2}-\frac{1}{\eta+k}\left(1-\frac{\partial\psi}{\partial\eta}\right)\right]\right\}=0 \tag{33}$$

$$\frac{1}{(k+\eta)}\frac{\partial}{\partial\eta}\left[(k+\eta)\frac{\partial\theta}{\partial\eta}\right]+\mathrm{Br}\left[a^*+(\Pi)^{n-1}\right]\left[-\frac{1}{k+\eta}\left(1-\frac{\partial\psi}{\partial\eta}\right)-\frac{\partial^2\psi}{\partial\eta^2}\right]^2=0 \tag{34}$$

Elimination of pressure between eqs. (25) and (33) yield:

$$\frac{\partial}{\partial\eta}\left\{\left(\frac{1}{(k+\eta)}\frac{\partial}{\partial\eta}\left\{(k+\eta)^2\left[a^*+(\Pi)^{n-1}\right]\right\}\right)\left[\frac{1}{k+\eta}\left(1-\frac{\partial\psi}{\partial\eta}\right)+\frac{\partial^2\psi}{\partial\eta^2}\right]\right\}=0 \tag{35}$$

The boundary conditions (16) and (17) transform to:

$$\psi=-\frac{q}{2},\ \frac{\partial\psi}{\partial\eta}=1,\ \theta=0,\ \phi=0,\ \text{at}\ \ \eta=h_1=1+\lambda\sin x \tag{36}$$

$$\psi=\frac{q}{2},\ \frac{\partial\psi}{\partial\eta}=1,\ \theta=1,\ \phi=1,\ \text{at}\ \ \eta=h_2=-1-\lambda\sin x \tag{37}$$

where $\lambda=b_1/a_1$ is the amplitude ratio.

The physical quantities of interest such as pressure rise per wavelength, Δp, heat transfer coefficients at both the wall $z_i(i=1,2)$ and Sherwood number at both the wall Sh_i $(i=1,2)$ are defined as [38] and [40]:

$$\Delta p=\int_0^{2\pi}\frac{\mathrm{d}p}{\mathrm{d}x}\mathrm{d}x \tag{38}$$

$$z_i=\frac{\partial h_i}{\partial x}\frac{\partial\theta}{\partial\eta}\bigg|_{\eta=h_i},\ \ i=1,\,2 \tag{39}$$

$$\mathrm{Sh}=\frac{\partial h_i}{\partial x}\frac{\partial\phi}{\partial\eta}\bigg|_{\eta=h_i},\ \ i=1,2 \tag{40}$$

Now, in order to solve eqs. (28), (34), and (35) one has to rely on suitable numerical method. This is because of strong non-linearity manifested by these equations. An implicit finite difference technique is employed for the solution.

Numerical solution of boundary value problem

In this section, we describe the finite difference method used for the solution of eqs. (28), (34), and (35) subject to boundary conditions given in eqs. (36) and (37). This procedure is based on following steps:

– The first step is to construct an iterative procedure in such a way that the original non-linear boundary value problem (BVP) is converted into a linear one at the $(m+1)^{\mathrm{th}}$ iterative step. For this particular problem, the following iterative procedure is proposed:

$$f(\eta+k)\frac{\partial^4\psi^{(m+1)}}{\partial\eta^4}+\left\{2\left[f+(\eta+k)\frac{\partial f}{\partial\eta}\right]\right\}\frac{\partial^3\psi^{(m+1)}}{\partial\eta^3}+\left[\frac{\partial f}{\partial\eta}+(\eta+k)\frac{\partial^2 f}{\partial\eta^2}-\frac{f}{\eta+k}\right]\frac{\partial^2\psi^{(m+1)}}{\partial\eta^2}+$$
$$+\left[\frac{f}{(\eta+k)^2}-\frac{1}{(\eta+k)}\frac{\partial f}{\partial\eta}-\frac{\partial^2 f}{\partial\eta^2}\right]\frac{\partial\psi^{(m+1)}}{\partial\eta}-\frac{f}{(\eta+k)^2}+\frac{1}{(\eta+k)}\frac{\partial f}{\partial\eta}+\frac{\partial^2 f}{\partial\eta^2}=0 \tag{41}$$

$$\frac{\partial^2\theta^{(m+1)}}{\partial\eta^2}+\frac{1}{\eta+k}\frac{\partial\theta^{(m+1)}}{\partial\eta}=-\mathrm{Br}\,f\left[-\frac{1}{k+\eta}\left(1-\frac{\partial\psi^{(m)}}{\partial\eta}\right)-\frac{\partial^2\psi^{(m)}}{\partial\eta^2}\right]^2 \tag{42}$$

$$\frac{\partial^2\phi^{(m+1)}}{\partial\eta^2}+\frac{1}{\eta+k}\frac{\partial\phi^{(m+1)}}{\partial\eta}=-\mathrm{Sr}\,\mathrm{Sc}\left[\frac{\partial^2\theta^{(m)}}{\partial\eta^2}+\frac{1}{(k+\eta)}\frac{\partial\theta^{(m)}}{\partial\eta}\right] \tag{43}$$

$$\psi^{m+1}=-\frac{q}{2},\ \ \frac{\partial\psi^{m+1}}{\partial\eta}=1,\ \ \theta^{(m+1)}=0,\ \ \phi^{(m+1)}=0\ \ \text{at}\ \ \eta=h_1, \tag{44}$$

$$\psi^{(m+1)}=\frac{q}{2},\ \ \frac{\partial\psi^{(m+1)}}{\partial\eta}=1,\ \ \theta^{(m+1)}=1,\ \ \phi^{(m+1)}=1\ \ \text{at}\ \ \eta=h_2, \tag{45}$$

where

$$f=a^*+\left[-\frac{\partial^2\psi^{(m)}}{\partial\eta^2}-\frac{1}{\eta+k}\left(1-\frac{\partial\psi^{(m)}}{\partial\eta}\right)\right]^{n-1}$$

Here the index (m) shows the iterative step. It is now clear that BVP is linear in $\psi^{(m+1)}$.

– At second step, we insert finite difference approximations of $\psi^{(m+1)}$, $\theta^{(m+1)}$, $\phi^{(m+1)}$, and their derivatives into eqs. (41)-(43). In this way, we get a system of linear algebraic equations at each iterative step.
– In third step, the system of algebraic equations obtained in previous step are solved at each cross-section to get numerical results of $\psi^{(m+1)}$, $\theta^{(m+1)}$, and $\phi^{(m+1)}$. Obviously, suitable initial guesses are required for $\psi^{(m)}$, $\theta^{(m)}$, and $\phi^{(m)}$ at each cross-section to start the iterative procedure. The iterative procedure at cross-section is carried out until a convergent solution is reached. To achieve convergent solution rapidly the method of successive under-relaxation is employed. In this method the values of $\tilde{\psi}^{(m+1)}$, $\tilde{\theta}^{(m+1)}$, and $\tilde{\phi}^{(m+1)}$ at $(m+1)^{\text{th}}$ iterative step are refined:

$$\psi^{(m+1)}=\psi^{(m)}+\tau\left[\tilde{\psi}^{(m+1)}-\psi^{(m)}\right]$$
$$\theta^{(m+1)}=\theta^{(m)}+\tau\left[\tilde{\theta}^{(m+1)}-\theta^{(m)}\right]$$
$$\phi^{(m+1)}=\phi^{(m)}+\tau\left[\tilde{\phi}^{(m+1)}-\phi^{(m)}\right]$$

where τ is under relaxation parameter. Usually τ is chosen small for rapid convergence. In present computation the iterative procedure is terminated after achieving the values of ψ, θ, and ϕ convergent to 10^{-8}. The described method is already used in the studies carried out by Wang *et al.* [45] and Ali *et al.* [47].

Computational results and interpretation

In this section, we interpret the computational results provided in figs. 2-21 to analyze some significant features of the peristaltic motion such as *flow characteristics, pumping characteristics, temperature distribution*, *mass concentration*, and *trapping phenomenon* for various values of the parameters k, n, a^*, Brinkman, Schmidt, and Sherwood numbers.

Figures 2 and 3 present the redial distribution of the transverse velocity u_2 for different values of a^* and n. Figure 2 shows for shear-thinning bio-fluids ($n < 1$) an increase in a^* accelerate the flow. The structure of axial velocity is also substantially affected with the increase in a^*. For smaller values of a^* the flow velocity is asymmetric with maximum in it appearing above $\eta = 0$. With increasing a^* to 1.5 the velocity approximately regained its symmetry. Larger values of a^* represent the case when viscous effects are stronger than the power-law effects. In such situation, the effects of curvature on axial velocity are not significant. However, as a^* decrease in value, the effects of curvature become dominant. Figure 3 illustrates the axial velocity profile for three different values of power-law index, n. It is observed that axial velocity increases with increasing n. For $n < 1$ (pesudoplastic/shear-thinning biofluids), the axial velocity exhibits a boundary-layer type character. However, such characteristic of axial velocity vanishes for Newtonian ($n = 0$) and shear-thinning/dilatant fluids. For such fluids, non-vanishing gradients in axial velocity occur in the whole flow span [$0, h$].

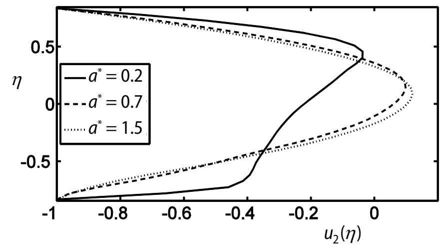

Figure 2. Variation of $u_2(\eta)$ for different values of a^* with $k = 3$, $n = 0.7$, $\lambda = 0.4$, and $\theta = 1.5$

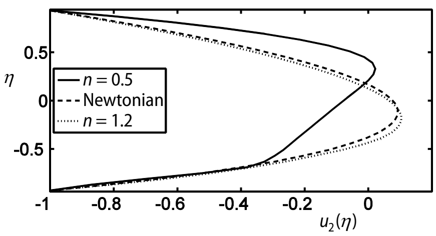

Figure 3. Variation of $u_2(\eta)$ for different values of n with $k = 2.5$, $a^* = 0.1$, $\lambda = 0.4$, and $\theta = 1.5$

The pressure rise per wavelength against flow rate is plotted in figs. 4-6 for different values of a^*, n, and k. Three distinct cases can be identified from these plots: peristaltic pumping case ($\Theta > 0$, $\Delta p > 0$), free pumping case ($\Theta > 0$, $\Delta p = 0$), and augmented pumping case ($\Theta > 0$, $\Delta p < 0$). It is observed that for peristaltic pumping case, the pressure rise per wavelength increases by increasing a^*, n, and k for a fixed value of Θ. This is consistent with observations already made for the axial velocity in figs. 2 and 3. For the case when $\Delta p = 0$ an increase in a^* does not significantly affect the magnitude of the flow rate Θ. However, the magnitude of Θ corresponding to $\Delta p = 0$ increases with increasing power-law index and channel curvature. In augmented pumping case, the flow due to peristalsis is assisted by the pressure gradient and the magnitude of assistance increase with increasing a^* and n. In contrast, the assistance provided by pressure gradient decreases with increasing k.

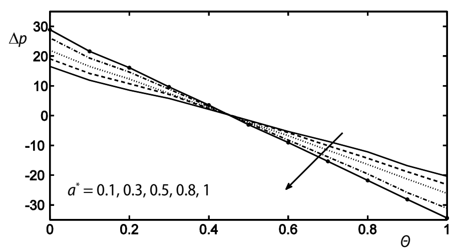

Figure 4. Variation of Δp for different values of a^* with $n = 0.7$, $\lambda = 0.4$, and $k = 2$

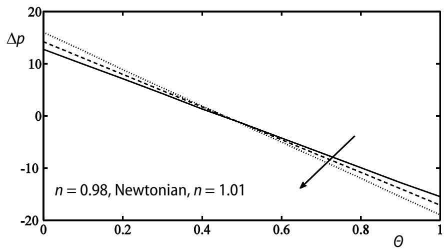

Figure 5. Variation of Δp for different values of n with $a^* = 0.1$, $\lambda = 0.4$, and $k = 2$

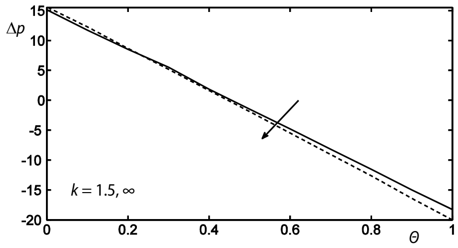

Figure 6. Variation of Δp for different values of k with n = 0.99, a^* = 0.1, and λ = 0.4

The effects of viscosity parameter, a^*, and Brinkman number on the temperature distribution inside the channel are graphically displayed in figs. 7 and 8 for shear thinning biofluid ($n < 1$). An enhancement in the temperature inside the channel is observed with increase in a^* and Brinkman number.

Figures 9 and 10 depict the effects of a^*, and Brinkman number on the heat transfer coefficient, z, at the upper wall. It is observed through both figures that the heat transfer coefficient varies periodically along the channel. This is in fact a direct consequence of the periodic nature of the peristaltic wall. Moreover, the amplitude of heat transfer coefficient enhances via increasing a^*, and Brinkman number. Figures 11-14 depict the behavior of the mass concentration, ϕ, for different values of a^*, Br, Sr, and Sc, respectively. These figures show that the concentration distribution is an increasing function of a^*, Br, Sr, and Sc.

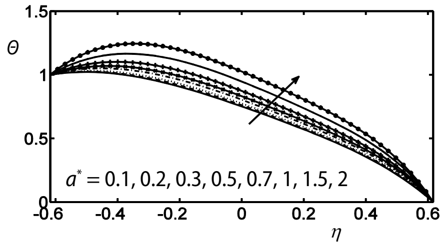

Figure 7. Profile of temperature $\theta(\eta)$ for different values of a^* with n = 0.95, Br = 0.5, λ = 0.4, and k = 2

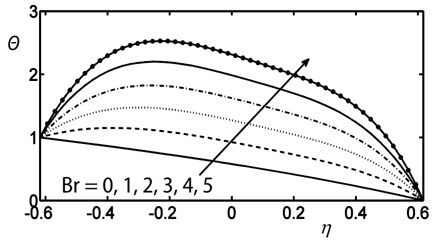

Figure 8. Profile of temperature $\theta(\eta)$ for different values of Br with n = 0.95, a^* = 0.1, λ = 0.4, and k = 2

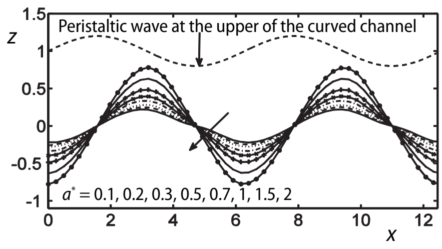

Figure 9. Variation of heat transfer coefficient, z, at upper wall for different values of a^* with n = 0.98, Br = 0.5, λ = 0.4, and k = 2

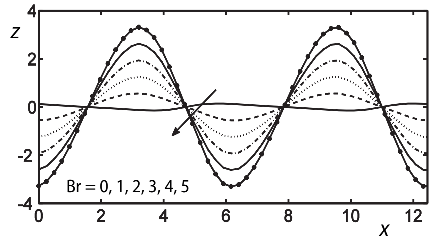

Figure 10. Variation of heat transfer coefficient, z, at upper wall for different values of Br with a^* = 0.1, n = 0.98, λ = 0.4, and k = 2

The impact of several parameters such as a^*, Br, Sr, and Sc on the Sherwood number at the upper wall is shown through figs. 15-18. Similar to the heat transfer coefficient, Sherwood number also oscillates periodically. Further, the amplitude of oscillations in Sherwood number enhance via increasing a^*, Br, Sr, and Sc.

An interesting feature of the peristaltic motion is known as trapping. Trapping is a phenomenon in which closed circulating streamlines exist at very high flow rates or for large occlusions ratios. The particular pattern of streamlines for three values of viscosity parameter, a^*, for *shear-thinning* fluid are shown in fig. 19. It is noticed that a circulating bolus of fluid

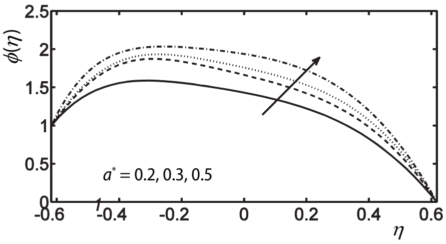

Figure 11. Variation of mass concentration, ϕ, for different values of a^* with n = 0.9, Br = 2, Sr = 1, Sc = 1, λ = 0.4, and k = 2

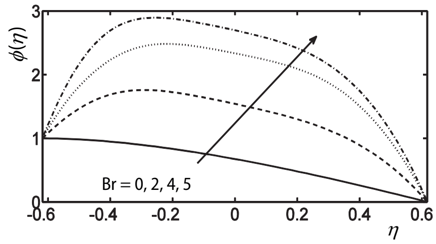

Figure 12. Variation of mass concentration, ϕ, for different values of Br with n = 0.9, a^* = 0.1, Sr = 1, Sc = 1, λ = 0.4, and k = 2

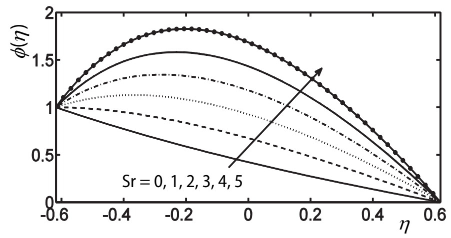

Figure 13. Variation of mass concentration, ϕ, for different values of Sr with n = 0.9, a^* = 0.1, Br = 2, Sc = 1, λ = 0.4, and k = 2

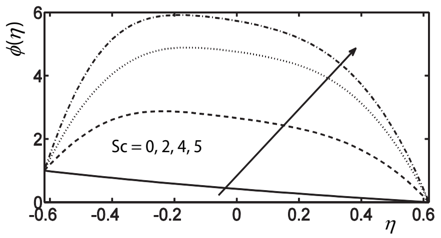

Figure 14. Variation of mass concentration, ϕ, for different values of Sc with n = 0.9, a^* = 0.1, Sr = 1, Br = 2, λ = 0.4, and k = 2

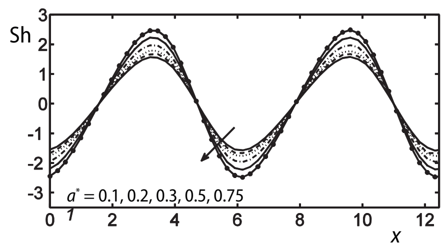

Figure 15. Variation of Sherwood number at upper wall for different values of a^* with n = 0.9, Br = 2, Sr = 1, Sc = 1, λ = 0.4, and k = 2

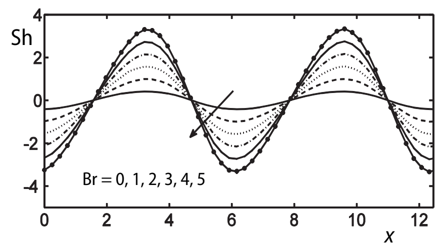

Figure 16. Variation of Sherwood number at upper wall for different values of Br with n = 0.98, a^* = 0.1, Sr = 1, Sc = 1, λ = 0.4, and k = 2

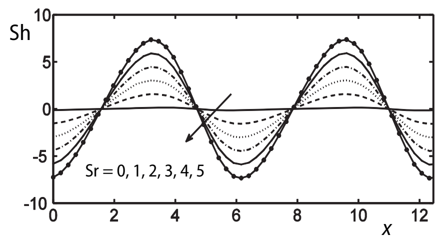

Figure 17. Variation of Sherwood number at upper wall for different values of Sr with n = 0.98, a^* = 0.1, Br = 2, Sc = 1, λ = 0.4, and k = 2

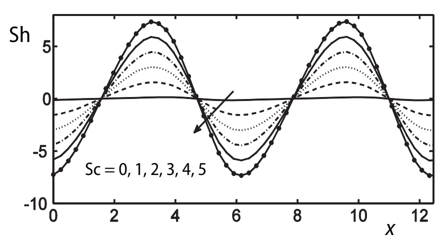

Figure 18. Variation of Sherwood number at upper wall for different values of Sc with n = 0.98, a^* = 0.1, Br = 2, Sr = 1, λ = 0.4, and k = 2

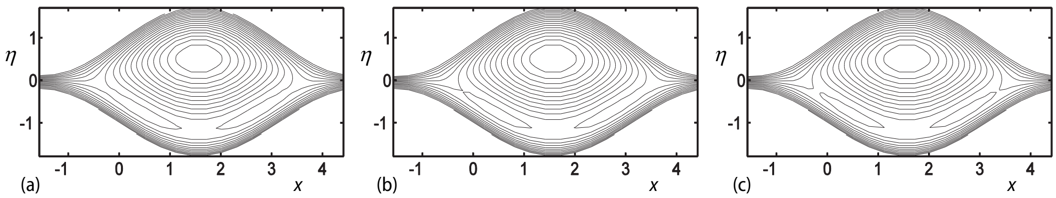

Figure 19. Streamlines in wave frame for (a) a^* = 0.1, (b) a^* = 0.98, and (c) a^* = 2, for n = 0.98. The other parameters chosen are k = 2, and λ = 0.4

concentrated in the upper half of the channel exists for a^* = 0.1. No significant change is observed by increasing a^* from 0.1 to 2, except the appearance of small eddies near the lower wall of the channel. The effects of power-law index, n, on streamlines pattern are shown in fig. 20 for a^* = 0.1. Figure 20 shows a circulating bolus of fluid concentrated in the lower part of the channel for shear-thinning fluid, $n \geq 0.9$. A small circulating eddy near the upper wall is also identified. The bolus shift towards the upper wall of the channel via increasing n from 0.98 to 1 *i. e.*, changing the behavior of the biofluid from *shear-thinning* to Newtonian fluids. A further rise in the value of (*power-law index*) n does not effect on the circulating phenomena in the upper part of the channel. However, a slight decrease in the size of eddy near the low wall is noted. The influence of channel curvature on trapping phenomena is illustrated through fig. 21. A circulating bolus of fluid concentrated in the upper part of the channel exists for $k = 2$. The bolus regain its symmetric shape as $k \rightarrow \infty$.

From the previous discussion it is concluded that the role of k is to affect the bolus symmetry while the effect of n is to shift the center of circulation from lower part of channel to the upper one.

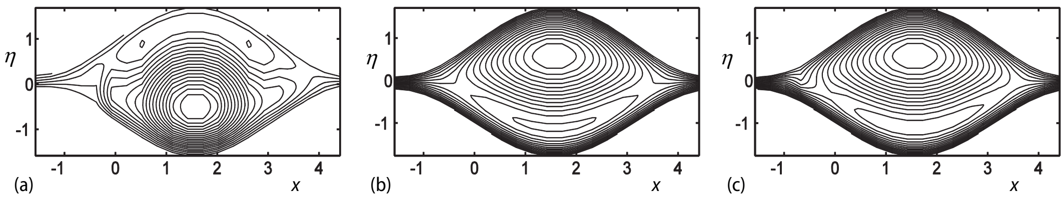

Figure 20. Streamlines in wave frame for (a) n = 0.9, (b) n = 1, and (c) n = 1.05, for k = 2.5. The other parameters chosen are a^* = 0.1, and λ = 0.4

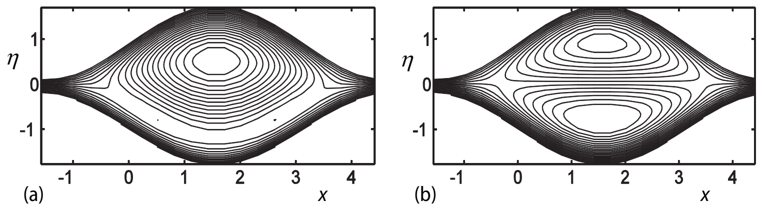

Figure 21. Streamlines in wave frame for (a) k = 2, and (b) k $\rightarrow \infty$, for n = 0.98. The other parameters chosen are a^* = 0.1, and λ = 0.4

Concluding remarks

A 2-D laminar incompressible flow of a Sisko fluid induced by peristalsis through a curved channel is investigated. The heat and mass transfer characteristics are also analyzed employing energy and concentration equations. Particular focus is given to effects of geometrical and rheological parameters of the model on flow and heat/mass characteristics. The dimensionless governing equations are solved with the well-tested, robust, highly efficient, implicit finite difference numerical method. Extensive computations and flow visualization are presented through graphs.

It is observed that the rheological and geometrical parameters significantly affect the peristaltic and heat/mass transfer phenomena. For strong shear-thinning biofluids a thin boundary-layer develops near the channel walls. Trapping phenomena is also largely altered by rheological parameters. Though viscosity parameter does not affect the circulating bolus in the upper wall of the channel but it creates two tiny eddies near the lower wall for strong shear-thinning biofluid. The circulating bolus shift from the upper half to lower half of the channel with a change in behavior of the fluid from *shear-thinning* to *shear thickening*. Both temperature and mass concentration profiles are strongly influenced by the involved parameters. Each of this physical quantity is found to increase with increasing a^* and Brinkman nuber. The heat transfer coefficient and Sherwood number oscillates periodically and their amplitudes are greatly enhanced with enhancing the numerical values of and a^* and Brinkman nuber.

Nomenclature

a^* – viscosity parameter, [kgm^{-1}s^{-1}]
a_1 – infinite shear-rate viscosity, [kgm^{-1}s^{-1}]
b – amplitude of wave, [m]
b_1 – consistency index, [Pas^n]
C – mass concentration, [kg]
c – wave speed, [ms^{-1}]
c_p – specific heat at constant pressure, [m^{2}s^{-2}K^{-1}]
D – coefficient of mass diffusivity, [m^{2}s^{-1}]
K_T – thermal diffusivity, []m^{2}s^{-1}]
k^* – thermal conductivity, [Wm^{-1}K^{-1}]
T – temperature, [K]
T_m – mean fluid temperature, [K]
u_1, u_2 – velocity component, [ms^{-1}]

Greek symbols

λ^* – wavelength, [m]
ρ – density, [kgm^{-3}]
Φ – dissipation function, [kgm^{-1}s^{-3}]

References

[1] Bandopadhyay, A., *et al*., Electroosmosis-Modulated Peristaltic Transport in Microfluidic Channel, *Phy. of Fluids, 28* (2016), 5, 052002
[2] Tripathi, D., *et al*., Transverse Magnetic Field Driven Modification in Unsteady Peristaltic Transport with Electrical Double Layer Effects, *Colloid Surface A*, *506* (2016), Oct., pp. 32-39
[3] Latham, T. W., Fluid Motion in Peristaltic Pump, M. Sc. thesis, MIT Press, Cambridge, Mass., USA, 1966
[4] Shapiro, A. H., *et al*., Peristaltic Pumping with Long Wavelength at Low Reynolds Number*, J. of Fluid Mech., 37* (1969), 4, pp. 799-825
[5] Fung, Y. C., Yih, C. S., Peristaltic Transport, *Trans. ASME Journal of App. Mech*., *35* (1968), 4, pp. 669-675
[6] Barton, C., Raynor, S., Peristaltic Flow in Ttubes, *The Bulletin of Math. Biophy., 30* (1968), 4, pp. 663-680
[7] Jaffrin, M. Y., Inertia and Streamline Curvature Effects in Peristaltic Pumping, *Int. J. of Eng. Sci., 11* (1973), 6, pp. 681-699
[8] Jaffrin, M. Y., Shapiro, A. H., Peristaltic Pumping, *Annual Review of Fluid Mech*., *3* (1971), Jan., pp. 13-37
[9] Mittra, T. K., Parsad, S. N., Interaction of Peristaltic Motion with Poiseuille Flow, *The Bulletin of Math. Bio., 36* (1974), Feb., pp. 127-141
[10] Srivastava, L. M., Srivastava, V. P., Interaction of Peristaltic Flow with Pulsatile Flow in a Circular Cylindrical Tube, *J. of Biomech., 18* (1985), 4, pp. 247-253
[11] Brown, T. D., Hung, T. K., Computational and Experimental Investigations of Two-Dimensional Nonlinear Peristaltic Flows, *J. of Fluid Mech., 83* (1977), 2, pp. 249-272
[12] Takabatake, S., Ayukawa, K., Numerical Study of Two-Dimensional Waves, *J. of Fluid Mech*., *22* (1982), 2, pp. 439-465
[13] Takabatake, S., *et al*., Peristaltic Pumping in Circular Cylindrical Tubes: a Numerical Study of Fluid Transport and its Efficiency, *J. of Fluid Mech*., *193* (1988), Aug., pp. 267-283
[14] Raju, K. K., Devanathan, R., Peristaltic Motion of Non-Newtonian Fluid, *Acta, 11* (1972), 2, pp. 170-178

[15] Raju, K. K., Devanathan, R., Peristaltic Motion of Non-Newtonian Fluid II, Viscoelastic Fluid Rheol, *Acta, 13* (1974), 6, pp. 944-948
[16] Siddiqui, A. M., *et al*., Peristaltic Pumping of Second Order Fluid in a Planar Channel, *Rheol. Acta*, *30* (1991), 3, pp. 249-262
[17] Siddiqui, A. M., Schwarz, W. H., Peristaltic Flow of Second Order Fluid in Tubes, *J. of Non-Newtonian Fluid Mech., 53* (1994), July, pp. 257-284
[18] Hayat, T., *et al*., Peristaltic Transport of Third Order Fluid in a Cylindrical Tube, *Math. Models and Methods in App. Sci., 12* (2002), 12, pp. 169-176
[19] Hayat, T., *et al*., Peristaltic Motion of Johnson-Segalman Fluid in a Planar Channel, *Math. Problems in Eng., 2003* (2003), 1, pp. 1-23
[20] Hayat, T., *et al*., Peristaltic Transport of an Oldroyd-B Fluid in a Planar Channel*, Math. Problems in Eng., 2004* (2004), 4, pp. 347-376
[21] Srinivasacharya, D., *et al*., Peristaltic Pumping of a Micropolar Fluid in a Tube, *Acta Mech*., *161* (2003), 3-4, pp. 165-178
[22] Mekheimer, Kh. S., Peristaltic Transport of a Newtonian Fluid through a Uniform and Non-Uniform Annulus, *The Arabian J. of Sci. and Eng., 30* (2005), 1, pp. 71-83
[23] Haroun, M. H., Nonlinear Peristaltic Flow of a Fourth Grade Fluid in an Inclined Asymmetric Channel, *Comp. Material Sci*., *39* (2007), 10, pp. 324-333
[24] Vajravelu, K., *et al*., Peristaltic Flow and Heat Transfer in a Vertical Porous Annulus with Long Wavelength Approximation, *Int. J. of Nonlinear Mech.*, *42* (2008), 5, pp. 754-759
[25] Tripathi, D., Beg, O. A., A Study of Unsteady Physiological Magneto-Fluid Flow and Heat Transfer through a Finite Length Channel by Peristaltic Pumping, *Proceedings,* Institution of Mechanical Engineers, Part H, *J. of Eng. in Med., 226* (2012), 8, pp. 631-644
[26] Tripathi, D., *et al*., Mathematical Modelling of Heat Transfer Effects on Swallowing Dynamics of Viscoelastic Food Bolus through the Human Oesophagus, *Int. J. of Thermal Sci*., *70* (2013), Aug., pp. 41-53
[27] Tripathi, D., Beg, O. A., Mathematical Modelling of Peristaltic Propulsion of Viscoplastic Bio-Fuids, *Proceedings,* Institution of Mechanical Engineers, Part H, *J. of Eng. in Med*., *228* (2014), 1, pp. 67-88
[28] Nabil, T. M., *et al*., Effects of Chemical Reaction with Heat and Mass Transfer on Peristaltic Flow of Jeffrey Fluid through Porous Medium in an Inclined Asymmetric Channel with Hall Currents, *International Journal of Applied Mathematics and Physics, 3* (2011), 2, pp. 155-167
[29] Tanveer, A., *et al*., Effects of the Cattaneo-Christov Heat Flux Model on Peristalsis, *Engineering Applications of Computational Fluid Mechanics, 10* (2016), 1, pp. 373-383
[30] Walker, S. W., Shelley, M. J., Shape Optimization of Peristaltic Pumping, *J. of Comp. Phy., 229* (2010), 4, pp. 1260-1291
[31] Ceniceros, H. D., Fisher, J. E., Peristaltic Pumping of a Viscoelastic Fluid at High Occlusion Ratios and Large Weissenberg Numbers, *J. of Non-Newtonian Fluid Mech*., *171-172* (2013), Mar., pp. 31-41
[32] Boehme, G., Mueller, A., Analysis of Non-Newtonian Effects in Peristaltic Pumping, *J. of Non-Newtonian Fluid Mech., 201* (2013), Nov., pp. 107-119
[33] Shit, G. C., Roy, M., Hydromagnetic Effect on Inclined Peristaltic Flow of a Couple Stress Fluid, *Alex. Eng. J., 53* (2014), 4, pp. 949-958
[34] Abbas, M. A., *et al*., Three Dimensional Peristaltic Flow of Hyperbolic Tangent Fluid in Non-Uniform Channel Having Flexible Walls, *Alexandria Engineering Journal, 55* (2016), 1, pp. 653-662
[35] Abbas, M. A., *et al*., Application of Drug Delivery in Magnetohydrodynamics Peristaltic Blood Flow of Nanofluid in a Non-Uniform Channel, *Journal of Mechanics in Medicine and Biology*, *16* (2016), 4, 1650052
[36] Abbas, M. A., *et al*., Analysis of Entropy Generation in the Flow of Peristaltic Nanofluids in Channels with Compliant Walls, *Entropy, 18* (2016), 3, 90
[37] Sato, H., *et al*., Two Dimensional Peristaltic Flow in Curved Channels, *The Japan Society of Mechanical Engineers*, *66* (2000), 643, pp. 679-685
[38] Ali, N., *et al*., Long Wavelength Flow Analysis in a Curved Channel, *Zeitschrift für Naturforsch, 65a* (2010), 3, pp. 191-196
[39] Hayat, T., *et al*., Peristaltic Transport of Carreau-Yasuda Fluid in a Curved Channel with Slip Effects, *PLos One*, *9* (2011), 4, pp. 5126-5136
[40] Ramanamurthy, J. V., *et al*., Unsteady Peristaltic Transport in Curved Channels, *Phy. of Fluids*, *25* (2013), 9, 091903
[41] Kalantari, A., *et al*., Peristaltic Flow of Non-Newtonian Fluids through Curved Channels: A Numerical Study, *Annual Transactions of the Nordic Rheo. Society, 21* (2013), pp. 163-170

[42] Ali, N., *et al*., Heat Transfer Analysis of Peristaltic Flow in a Curved Channel, *Int. J. of Heat and Mass Trans*., *53* (2010), 15-16, pp. 3319-3325
[43] Hayat, T., *et al*., Effect of Wall Properties on the Peristaltic Fow of a Third Grade Fuid in a Curved Channel with Heat and Mass Transfer, *Int. J. of Heat and Mass Trans*., *54* (2011), 23-24, pp. 5126-5136
[44] Hina, S., *et al*., Heat and Mass Transfer Effects on the Peristaltic Flow of Johnson-Segalman Fluid in a Curved Channel with Compliant Walls, *Int. J. of Heat and Mass Trans., 55* (2012), 13-14, pp. 3511-3521
[45] Wang, Y., *et al*., Magneto Hydrodynamic Peristaltic Motion of a Sisko Fluid in a Symmetric or Asymmetric Channel, *Phy. A, 387* (2008), 2-3, pp. 347-362
[46] Ali, N., *et al*., New Concept about Existence of Hartmann Boundary Layer in Peristalsis Through Curved Channel-Asymptotic Solution, *Meccanica*, *51* (2016), 8, pp. 1783-1795
[47] Ali, N., *et al*., Slip Effects on the Peristaltic Flow of a Third Grade Fluid in a Circular Cylindrical Tube, *J. of App. Mech., 76* (2009), 1, pp. 1-10

Paper submitted: October 18, 2016
Paper revised: April 7, 2017
Paper accepted: April 11, 2017